著者	論文タイトル	掲載誌名	巻 頁	出版年
Koide Y, Morikawa S, Mabuchi Y, Muguruma Y, Hiratsu E, Hasegawa K, Kobayashi M, Ando K, Kinjo K, Okano H, Matsuzaki Y.	Two distinct stem cell lineages in murine bone marrow.	Stem Cells	25 1213-1221	2007
K. Kadoyama, H. Funakoshi, W. Ohya, and T. Nakamura	Hepatocyte growth factor (HGF) attenuates gliosis and motoneuronal degeneration in the brainstem motor nuclei of a transgenic mouse model of ALS	Neurosci. Res	59 446-456	2007
A. Ishigaki, M. Aoki, M. Nagai, H. Warita, S. Kato, M. Kato, T. Nakamura, H. Funakoshi, and Y. Itoyama	Intrathecal Delivery of Hepatocyte Growth Factor From Amyotrophic Lateral Sclerosis Onset Suppresses Disease Progression in Rat Amyotrophic Lateral Sclerosis Model	J. Neuropathol. Exp. Neurol	66 1037-1044	2007
W. Ohya, H. Funakoshi, T. Kurosawa, and T. Nakamura	Hepatocyte growth factor (HGF) promotes oligodendrocyte progenitor cell proliferation and inhibits its differentiation during postnatal development in the rat.	Brain Res	1147 51-65	2007
M. Nakano, N. Takagi, K. Takagi, H. Funakoshi, K. Matsumoto, T. Nakamura, and S. Takeo	Hepatocyte growth factor promotes the number of PSD-95 clusters in young hippocampal neurons.	Exp. Neurol	207 195-202	2007
K. Kitamura, A. Iwanami, M. Nakamura, J. Yamane, K. Watanabe, Y. Suzuki, D. Miyazawa, S. Shibata, H. Funakoshi, S. Miyatake, R.S. Coffin, T. Nakamura, Y. Toyama, and H. Okano	Hepatocyte growth factor promotes endogenous repair and functional recovery after spinal cord injury.	J. Neurosci. Res	85 2332-2342	2007

著者	論文タイトル	掲載誌名	巻 頁	出版年
Kato S	Amyotrophic lateral sclerosis models and human neuropathology: similarities and differences.	Acta Neuropathol	115 97-114	2008
Suzuki M, Sugimoto Y, Ohsaki Y, Ueno M, Kato S, Kitamura Y, Hosokawa H, Davies JP, Ioannou YA, Vanier MT, Ohno K, Ninomiya H	Endosomal accumulation of Toll-like receptor 4 causes constitutive secretion of cytokines and activation of signal transducers and activators in Niemann-Pick disease type C (NPC) fibroblasts: a potential basis for glial cell activation in the NPC brain.	J Neuroscience	27 1879-1891	2007
Kitamura Y, Okazaki T, Nagatsuka Y, Hirabayashi Y, Kato S, Hayashi K	Immunohistochemical distribution of phosphatidylglucoside using anti-phosphatidylglucoside monoclonal antibody (DIM21).	Biochem Biophys Res Commun	362 252-255	2007
Fujiwara N, Nakano M, Kato S, Yoshihara D, Ookawara T, Eguchi H, Taniguchi N, Sizuki K	Oxidative modification to cysteine sulfonic acid of cys111 in human copper-zinc superoxide dismutase.	J Biol Chem; Online Publish	282 35933-35944	2007

著者	論文タイトル	掲載誌名	巻 頁	出版年
Masaya Nakamura	Electrical stimulation modulates fate determination of differentiating embryonic stem cells.	Stem Cells	25 562-570	2007
Masaya Nakamura	Plasma as a scaffold for regeneration of neural precursor cells after transplantation into rats with spinal cord injury.	Cell Transplant	16 57-65	2007
Masaya Nakamura	Establishment of Three-dimensional culture of neural stem/progenitor cells in collagen type-1 gel.	Rest Neurol Neurosci	25 109-117	2007
Masaya Nakamura	In vivo tracing of neural tracts in the intact and injured spinal cord of marmosets by diffusion tensor tractography.	J Neurosci	27 44-448	2007
Masaya Nakamura	Isolation and characterization of dendritic cells from common marmosets for preclinical studies on cell therapy.	Immunology		(in press)
Masaya Nakamura	Guidelines for the conduct of clinical trials for spinal cord injur as developed by the ICCP panel	Spinal Cord	45 190-205	2007
Masaya Nakamura	Guidelines for the conduct of clinical trials for spinal cord injury as developed by the ICCP panel: clinical trial outcome measures.	Spinal Cord	45 206-221	2007
Masaya Nakamura	Regenertion based therapies for spinal cord injuries.	Neurochem Int	51 68-73	2007

著者	論文タイトル	掲載誌名	巻 頁	出版年
中村雅也	Hepatocyte Growth Factor (HGF)を用いた脊髄損傷治療戦略　-新たな治療法の確立に向けて	関節外科	27(2) 185-194	2008
中村雅也	中枢神経の機能再建　細胞治療と人工臓器　　臨床応用をめざす脊髄再生	Midical Bio	4-49-55	2007
中村雅也	Semaphorin 3A選択的阻害剤による損傷脊髄の再生および運動機能回復の促進	実験医学	25 1221-1225	2007
中村雅也	脊髄損傷に対する再生医療の臨床治験はどこまで進んでいるか　-世界の動向とデーターについて	脊椎脊髄	20(12) 1224-1231	2007
中村雅也	Hepatocyte Growth Factor (HGF)を用いた脊髄損傷治療戦略	脊椎脊髄	20(12) 1239-1246	2007
中村雅也	脊髄損傷修復における反応性アストロサイトの役割	脳	10 134-138	2007
Kitamura K, Nakamura M et al	Hepatocyte growth factor promotes endogenous repair and functional recovery after spinal cord injury.	J Neursci Res	85 2332-2342	2007
Fujiyoshi K, Nakamura M et al	In vivo tracing of neural tracts in the intact and injured spinal cord of marmosets by diffusion tensor tractography.	J Neurosci	27 44-448	2007
Okano H, Nakamura M et al	Regenertion　based therapies for spinal cord injuries.	Neurochem Int	51 68-73	2007

著者	論文タイトル	掲載誌名	巻 頁	出版年
船越 洋、大谷 若菜、角 山 圭一、中村 敏一	ALSに対する新しい治療薬として肝細胞増殖因子（HGF）の研究	難病と在宅ケア	13 (7): 54-55	2007
船越 洋、大谷 若菜、角 山 圭一、中村 敏一	ALSと神経栄養因子—新規神経栄養因子・神経再生因子としてのHGF	Brain and Nerve （旧称：神経研究の進歩）	59 (10) 1195-1202	2007
船越 洋、角山 圭一、大 谷 若菜、中村 敏一	HGFの神経保護作用機序	Clinical Neurosci	25 620-621	2007
船越 洋、角山 圭一、大 谷 若菜、中村 敏一	HGFの神経疾患治療効果	Clinical Neurosci	25 500-501	2007
H. Akita, N. Takagi, N. Ishihara, K. Takagi, K. Murotomi, H. Funakoshi, K. Matsumoto, T. Nakamura, and S. Takeo	Hepatocyte growth factor improves synaptic localization of the NMDA receptor and intracellular signaling after excitotoxic injury in cultured hippocampal neuron.	Exp. Neurol	210 83-94	in press
Y. Suzuki, H. Funakoshi, M. Machide, K. Matsumoto, and T. Nakamura	Regulation of cell migration and cytokine production by HGF-like protein (HLP)/macrophage stimulating protein (MSP) in primary microglia.	Biomed. Res	29	in press

総説

著者	論文タイトル	掲載誌名	巻 頁	出版年
糸山　泰人	筋萎縮性側索硬化症の新規治療法開発への挑戦	神経治療学	24 607～614	2007

書籍

著者	論文タイトル	書籍全体の 編集者	書籍名	出版社	巻 頁	出版年
船越 洋、金井 将昭、 中村 敏一	神経栄養因子の多様な機能と神経変性疾患への臨床適用の可能性	高橋 良輔	神経変性疾患のサイエンス	南光堂	217-226	2007

J Neuropathol Exp Neurol

Vol. 66, No. 6
June 2007
pp. 517–524

ORIGINAL ARTICLE

Motor Neuron Disease in Transgenic Mice With an H46R Mutant *SOD1* Gene

Shoichi Sasaki, MD, Makiko Nagai, MD, Masashi Aoki, MD, Takashi Komori, MD, Yasuto Itoyama, MD, and Makoto Iwata, MD

Abstract

Human familial amyotrophic lateral sclerosis with an H46R mutant Cu/Zn superoxide dismutase (*SOD1*) gene is characterized by initial muscle weakness and atrophy in the legs and a very long-term clinical course (approximately 15 years). Transgenic mice with this mutation generated in our laboratory occasionally showed aggregates in the anterior horns and axonal degeneration in all white matter sections of the spinal cord on plastic sections at the presymptomatic stages (12 and 16 weeks old), although conventional staining revealed no pathologic changes. At the symptomatic stages (20 and 24 weeks), loss of anterior horn neurons was observed. On plastic sections, aggregates were frequently seen not only in the anterior horns but also in the posterior horns and in all sections of white matter. Degenerated fibers were observed in the anterior and posterior roots as well as in white matter. Electron and immunoelectron microscopic observation revealed human *SOD1*- and ubiquitin-positive aggregates consisting of intermediate filaments in the anterior horn even from an early presymptomatic stage. Thus, H46R mutant *SOD1* transgenic mice are characterized by widespread pathologic changes of the spinal cord that extend beyond the motor system, including many aggregates lacking vacuoles. The close pathologic similarity makes this animal model suitable for the investigation of human familial amyotrophic lateral sclerosis with the mutation.

Key Words: Aggregates, Amyotrophic lateral sclerosis, Cu/Zn superoxide dismutase (*SOD1*), H46R, Mice, Motor neuron disease, Transgenic.

INTRODUCTION

Since the initial report of Cu/Zn superoxide dismutase (*SOD1*) mutation involvement in familial amyotrophic lateral sclerosis (FALS), more than 100 mutations on all 5 exons of *SOD1* have been identified (1). Of the more than 100 mutations in humans, 3 mutant *SOD1* transgenic (Tg) mice (G85R, G37R, and G93A) have been extensively characterized as Tg mouse models of FALS (2, 3). Unlike the variable pattern of weakness in humans, weakness typically starts in the hindlimbs in mice between 3 and 12 months of age, depending on both the mutation and the level to which it is expressed. On the other hand, FALS with a novel point mutation (A to G, which results in an amino acid substitution of histidine-46 by arginine, H46R) in exon 2 of the *SOD1* gene is autosomal dominant and has been reported in the Japanese population. It has some characteristic clinical manifestations: initial development of muscle weakness and atrophy in the lower extremities; a very slow progression of symptoms to the upper extremities; and bulbar muscles with intrafamilial variation of disease severity. To a lesser extent, pyramidal signs also develop. The average age at onset is approximately 40 to 50 years, and the mean disease duration is about 15 years (4–6). In 1 study, the mean ± SD age at the onset in 1 family is 49.6 ± 10.9 years (n = 10) and duration after the onset is 17.3 ± 10.7 years (n = 4), and in another family durations are 48 ± 9.5 (n = 14) and 16.8 ± 6.8 years (n = 9), respectively (4). In another study, the disease duration of the family is 17.8 ± 13.2 years with the age at onset being 42.9 ± 4.7 years (n = 7) (5). In a third study, the average ± SD age at disease onset in the families is 44.3 ± 8.7 years (n = 17), and the mean disease duration is 12.0 ± 7.6 years (n = 17), with a range of 6 to 30 years (6). These clinical characteristics are reminiscent of the "pseudo-polyneuritic form" of amyotrophic lateral sclerosis (Marie-Patrikios-type) (7). To date, no studies of pathologic changes in H46R Tg mice have been reported, but there is a report of an H46R mutant *SOD1* Tg rat (8). The spinal cords of Tg mice with the H46R mutant *SOD1* gene were examined from the presymptomatic to symptomatic stages, and the findings were compared with cases of human FALS with the H46R mutant *SOD1* gene.

MATERIALS AND METHODS

Experimental Animals and Clinical Assessment

All mice were handled according to approved animal protocols of the Tohoku University Graduate School of Medicine.

From the Department of Neurology, Neurological Institute (SS, MI), Tokyo Women's Medical University, Tokyo, Japan; Department of Neurology (MN, MA, YI), Tohoku University Graduate School of Medicine, Sendai, Japan; and Department of Clinical Neuropathology (TK), Tokyo Metropolitan Institute for Neuroscience, Tokyo, Japan.

Send correspondence and reprint requests to: Shoichi Sasaki, MD, Department of Neurology, Neurological Institute, Tokyo Women's Medical University, 8-1 Kawada-cho, Shinjuku-ku, Tokyo 162-8666, Japan; E-mail: ssasaki@nij.twmu.ac.jp

This work was supported by a Grant-in-Aid for General Scientific Research (C) from the Japanese Ministry of Education, Science and Culture; a grant from the Japan ALS Association; and grants from the Ministry of Health, Labor and Welfare in Japan.

We isolated a P1-derived artificial clone (dJ100A14) containing the full genomic human *SOD1* gene. This clone was identified by screening a human genomic PAC library (9) using polymerase chain reaction with primer pairs specific to the human *SOD1* gene. From this, we cloned an 11.5-kilobase (kb) EcoRI-BamHI fragment that contained the entire coding sequence and promoter region of the human *SOD1* gene (10, 11). The H46R mutation was engineered into this fragment by site-directed mutagenesis (Mutan-express Km, Takara, Otsu, Japan). To obtain the H46R mutation, an NdeI-XbaI fragment involving the second exon was subcloned into the pKF18k vector. Both the mutagenic primer and selection primer, which restored Km resistance, were hybridized to the vector and were incorporated during replication. The resulting potential Km-resistant clones were sequenced by the oligonucleotide-directed dual amber method (12) to verify the presence of the introduced mutation, H46R. A linear 11.5-kb EcoRI-BamHI fragment containing the H46R mutation was microinjected into BDF1 (C57BL/6 × DBA/2 F1) mouse (The Jackson Laboratory, Bar Harbor, ME) embryos. The treated embryos were transferred to oviducts of pseudopregnant ICR-slc female mice.

The DNA of newborn mice was extracted from their tails for human *SOD1* gene-specific polymerase chain reaction amplification (forward primer: 5'-TTGGGAG GAGGTAGTGATTA; reverse primer: 5'-AGCTAGCAG GATAACAGATGA; 94°C for 30 seconds; 55°C for 30 seconds; 72°C for 30 seconds; 30 cycles). Founder mice were mated with C57B/6 mice (The Jackson Laboratory).

To generate Tg mice with the H46R mutation, we first obtained human genomic PAC clones encompassing the entire human *SOD1* gene; we then subcloned this gene within an 11.5-kb EcoRI-BamHI fragment. Site-directed mutagenesis was used to generate clones with the H46R mutation. The mutated 11.5-kb EcoRI-BamHI fragments were microinjected into fertilized eggs from BDF1 mice. Eighty-three potential Tg H46R pups were obtained. From these, 3 founders with the H46R mutant transgene were identified using polymerase chain reaction and Southern blotting. One line with the H46R mutation developed motor neuron disease. This line expressed the highest level of the mutant *SOD1*.

To determine the level of the human mutant *SOD1* protein that accumulated in the Tg line, spinal cord extracts were immunoblotted. The ratios of human mutant to mouse endogenous *SOD1* were determined using an anti-human polyclonal antibody against a peptide sequence identical in human and mouse *SOD1* (Calbiochem, San Diego, CA). The level of human mutant *SOD1* protein in the line H46R-70 was 20.1 times the level of endogenous mouse *SOD1*. To determine the level of *SOD1* activity, spinal cord extracts of Tg mice as well as those of controls were electrophoresed in native gels. *SOD1* activity was quantified in situ on the gels using a well-established assay system in which dismutation of superoxide anion by *SOD1* inhibits the conversion by superoxide anion of nitro blue tetrazolium to formazan, resulting in a formazan-free clear zone in an otherwise blue gel (13). The level of *SOD1* activity in the H46R-70 line was 20% of the control level.

The first sign of disease in this mutant line was weakness of limbs, primarily indicated by the dragging of 1 limb. In the H46R-70 line, all of the mice showed weakness in their hindlimbs. The mean age at which this clinical weakness appeared in the H46R-70 line was 153 ± 10.0 days (n = 4). As the disease progressed, the mice exhibited marked muscle wasting in their limbs. Thereafter, the other limbs also became weak. At the end stage of disease, the affected mice were unable to move toward water to drink and they died. The mean ages at death in the H46R-70 line were 184 ± 11.8 days (n = 4). The mean duration of the clinical expression of the disease in the H46R-70 was 27.5 ± 8.2 days (n = 4). The lines that expressed lower levels of human mutant *SOD1* did not show any clinical phenotypes at 12 months of age.

Histopathology

A total of 8 Tg mice and 8 age-matched nontransgenic (non-Tg) mice were investigated, respectively. Eight Tg mice were divided into 4 groups: early presymptomatic (aged 12 weeks, n = 2), late presymptomatic (16 weeks, n = 2), early symptomatic (20 weeks, n = 2), and end-stage Tg mice (24 weeks, n = 2). Age-matched non-Tg mice served as controls in each group (n = 8). Tg and non-Tg mice were examined simultaneously. All mice (n = 16) were deeply anesthetized with ether and perfused intracardially with heparinized saline (pH 7.4), followed by perfusion with ice-cold 4% paraformaldehyde (Katayama Chemical, Osaka, Japan) in 0.1 M phosphate buffer (pH 7.4). The spinal cord was removed rapidly and post-fixed by immersion in the same fixative (5 days, 4°C). Cross-sections of the spinal cord were embedded in paraffin, sectioned (4 μm), and subsequently stained with hematoxylin and eosin (H&E) and Klüver-Barrera stain.

Immunohistochemistry

The following antibodies were used in this study: a sheep polyclonal anti-human *SOD1* antibody (Calbiochem; diluted 1:1,000), a polyclonal anti-ubiquitin antibody (diluted 1:10; Sigma), a polyclonal anti-glial fibrillary acidic protein (GFAP) antibody (diluted 1:750; DAKO, Glostrup, Denmark), a mouse monoclonal antibody to rat phosphorylated neurofilament (SMI-31, diluted 1:1000; Sternberger Monoclonals, Lutherville, MD), a polyclonal antibody against a synthetic peptide corresponding to amino acid residues 124 to 134 of human α-synuclein with phosphoserine 129 (PSer 129, diluted 1:1000; a gift from Dr. T. Iwatsubo [14]), and a mouse monoclonal phosphorylated tau (AT8) (diluted 1:1000; Innogenetics, Ghent, Belgium). Sections (4-μm-thick) of the paraffin-embedded spinal cords were deparaffinized and treated with nonimmune serum as the blocking reagent, and the reaction was quenched with 3% H_2O_2. The samples were then incubated overnight at 4°C with the primary antibodies. Antibody binding was visualized by the avidin-biotin-immunoperoxidase complex (ABC) method using an Elite ABC kit (Vector Laboratories, Burlingame, CA) following the manufacturer's recommendations. 3,3'-diaminobenzidine tetrahydrochloride was the final chromogen. Selected sections were incubated with the antibodies against phosphorylated neurofilament, ubiquitin, and *SOD1* that had been preabsorbed with excess amounts of

these antibodies. Sections from which the primary antibodies had been omitted served as negative reaction controls.

Electron Microscopy

Eight Tg and 8 non-Tg wild-type mice were killed at ages 12, 16, 20, and 24 weeks (n = 2 in each group, respectively). All mice were perfused intracardially with heparinized saline (pH 7.4) followed by perfusion with ice-cold 4% paraformaldehyde (Katayama Chemical, Osaka, Japan) and 0.2% glutaraldehyde in 0.1 M phosphate buffer (pH 7.4). Tissues of the spinal cord were incubated in 2% osmium tetroxide in 0.1 M cacodylate for 2 hours, washed, dehydrated, and embedded in epoxy resin. Serial semithin sections (1 μm) of the whole transverse spinal cord stained with toluidine blue were examined under a light microscope. Appropriate portions were cut into ultrathin sections, which were subsequently stained with lead citrate and uranyl acetate for electron microscopic study.

Immunoelectron Microscopy

Postembedding immunogold electron microscopy was carried out on spinal cord specimens. Late presymptomatic (16 weeks, n = 1), early symptomatic (20 weeks, n = 1), and end-stage (24 weeks, n = 1) mice were perfused intracardially with heparinized saline (pH 7.4) followed by 100 mM phosphate buffer (pH 7.4) containing ice-cold 4% paraformaldehyde and 0.1% glutaraldehyde. Two non-Tg wild-type mice (20 weeks, n = 1; 24 weeks, n = 1) served as controls. The lumbar and cervical spinal cord from fixed mice were dissected out, dehydrated in 100% ethanol, and embedded in hard-grade LR White resin (Electron Microscopy Sciences, Fort Washington, PA) by polymerization overnight at 60°C. Ultrathin sections were excised from the embedded tissue using a microtome, and the sections were collected onto grids (150 mesh). Then, the ultrathin sections were etched in 0.1 N HCl for 5 minutes, rinsed 3 times for 5 minutes each in Tris-buffered saline (TBS) (20 mM Tris, 140 mM NaCl, and 2.7 mM KCl, pH 8.0), treated with blocking buffer (0.1% gelatin, 1% normal goat serum, and 0.3% Triton-X-100 in TBS) for 30 minutes, incubated with the primary antibodies for 2 hours at room temperature, rinsed 3 times for 5 minutes each in TBS, placed in gold-conjugated secondary antibody (10 nm gold anti-mouse anti-rabbit) for 1 hour, rinsed 3 times in TBS, rinsed in water, stained with Reynold's lead citrate followed by staining with aqueous 2% uranyl acetate, and then dried on filter paper. The following antibodies and sera were used: a sheep polyclonal anti-human *SOD1* antibody at 1:500, 1:1000, or 1:2000 (Calbiochem) dilution; a polyclonal anti-ubiquitin antibody (DAKO) diluted at 1:100, 1:500, or 1:1000; a monoclonal anti-phosphorylated neurofilament antibody (DAKO) diluted at 1:50, 1:100, 1:500, and normal rabbit serum (Vector Laboratories).

RESULTS

Light Microscopic Findings

In 12-week-old mice (early presymptomatic stage) the H&E and Klüver-Barrera staining revealed no pathologic changes such as vacuolar changes or neuronal loss anywhere in the spinal cord (Fig. 1A). The average number of large anterior horn neurons, which measured more than 18 μm in diameter (i.e. the mean of the shortest and the largest diameters of an anterior horn cell) per anterior horn was 15.7 ± 1.2 (n = 6 sections); thus, no significant differences from controls were observed in the experimental mice by either staining (H&E or Klüver-Barrera) or by neuronal count and measurement at this stage. Furthermore, no Lewy body-like inclusions (LIs) were observed anywhere in the samples by H&E staining. However, on Epon-embedded plastic sections stained with toluidine blue, rare aggregates and LIs were detected in the neuropil of the anterior horns and around the central canal, but not in the posterior horns or white matter. The anterior and posterior roots showed no abnormalities.

In 16-week-old mice (late presymptomatic stage), H&E and Klüver-Barrera staining revealed no pathologic changes in either the gray matter or the white matter. Aggregates and LIs were rarely observed by H&E staining. The average number of anterior horn neurons was 14.2 ± 1.5 (n = 6 sections), showing no significant difference from the controls. On plastic sections, occasional aggregates and LIs were seen in the neuropil in the anterior horns, as were spheroids and cord-like swollen axons (Fig. 2A). LIs

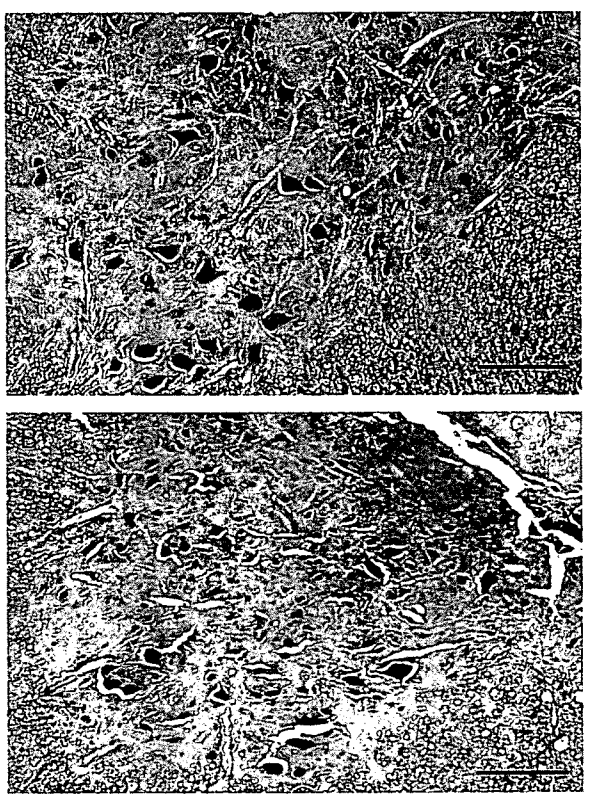

FIGURE 1. Cervical cord. **(A)** Anterior horn neurons are well preserved at the age of 12 weeks (early presymptomatic stage). Hematoxylin and eosin (H&E) staining. **(B)** Large anterior horn neurons are reduced at the age of 20 weeks (early symptomatic stage). H&E staining. Scale bars = 100 μm.

frequently contained cores at the center. Myelin ovoids were only occasionally observed in all white matter examined, but the anterior and posterior roots were intact.

In 20-week-old mice (early symptomatic stage), loss of anterior horn neurons with astrogliosis was observed, and the average number of large anterior horn neurons was

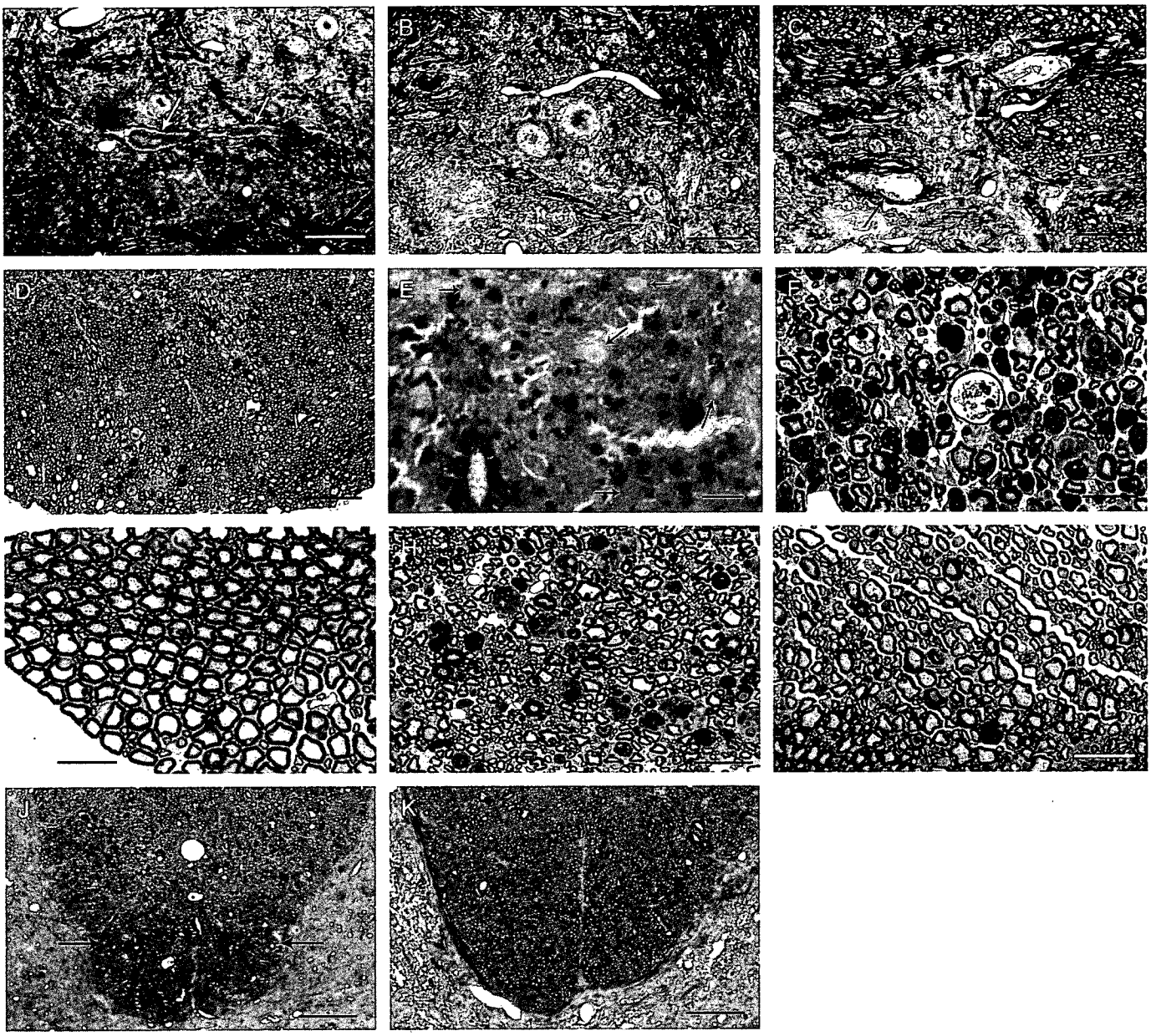

FIGURE 2. **(A)** Aggregates are observed in the cord-like swollen axon (arrows) at the age of 16 weeks (late presymptomatic stage) (lumbar cord). Plastic section stained by toluidine blue. **(B)** A Lewy body-like inclusion (arrow) is observed in the neuropil of the anterior horn at the early symptomatic stage (lumbar cord). Plastic section stained by toluidine blue. **(C)** Spheroids (arrows) are observed in the neuropil of the anterior horn and in the white matter close to the grey matter of the anterior horn at the early symptomatic stage (lumbar cord). Plastic section stained by toluidine blue. **(D)** Myelin ovoids are spotted in the anterior column at the early symptomatic stage (lumbar cord). Plastic section stained by toluidine blue. **(E)** Many aggregates or Lewy body-like inclusions (arrows) are observed in the neuropil of the anterior horn at the age of 24 weeks (end-stage) (cervical cord). Hematoxylin and eosin (H&E) staining. **(F)** Myelin ovoids are observed in the anterior root at the endstage (lumbar cord). Plastic section stained by toluidine blue. **(G)** A normal anterior root shown for comparison. Plastic section stained by toluidine blue. **(H)** Myelin ovoids are observed in the posterior root at the end stage (lumbar cord). Plastic section stained by toluidine blue. **(I)** A normal posterior root shown for comparison. Plastic section stained by toluidine blue. **(J)** Myelin ovoids are observed in the posterior column including the corticospinal tract (arrows) at the end stage (lumbar cord). Plastic section stained by toluidine blue. **(K)** A normal posterior column shown for comparison. Plastic section stained by toluidine blue. Scale bars = **(A–C)** 25 μm; **(D)** 50 μm; **(E–G)** 25 μm; **(H, I)** 30 μm; **(J, K)** 75 μm.

6.0 ± 1.4 (n = 6 sections), which was significantly fewer than that of the controls ($p < 0.01$) (Fig. 1B). Aggregates and LIs were occasionally observed in the anterior horn by H&E staining. On plastic sections, LIs (Fig. 2B), spheroids, and cord-like swollen axons were frequently seen in the neuropil of anterior horns (Fig. 2C). The white matter exhibited slight myelin ovoid formation in the anterior, lateral, and posterior columns (Fig. 2D). The anterior roots showed slight myelin ovoids, whereas the posterior roots were free of myelin ovoids.

In 24-week-old mice (end stage), loss of anterior horn neurons accompanied by astrogliosis was remarkable. The average number of anterior horn neurons was 4.8 ± 1.5 (n = 6 sections). Aggregates and LIs were frequently observed in the neuropil of the anterior horn by H&E staining (Fig. 2E). On the plastic sections, LIs were frequently seen both in the neuropil and in the cord-like swollen axons of the anterior horns; moreover, LIs were also observed in the posterior horns and in the white matter of the anterior, lateral, and posterior columns. Swollen axons (spheroids) were prominent in the exit zone of the anterior roots in the anterior columns as well as in the anterior horns. Myelin ovoids and degenerated fibers were prominent in the anterior roots (Fig. 2F, G) and posterior roots (Fig. 2H, I), as well as in the white matter of the anterior, lateral, and posterior columns, including the pyramidal tract (Fig. 2J, K). No vacuolar changes were observed anywhere at any stage.

Immunohistochemical Findings

In mice at the early presymptomatic stage of disease, *SOD1*- and ubiquitin-positive granular and linear deposits were only occasionally found in the neuropils of the anterior horns. No immunohistochemical abnormalities were revealed by antiphosphorylated neurofilament or GFAP antibodies, either in the gray or the white matter.

In mice at the late presymptomatic stage, many more *SOD1*- and ubiquitin-positive aggregates and LIs were observed in the neuropils of the anterior horns than at the previous stage of disease. Phosphorylated neurofilament-positive spheroids were only occasionally observed in the anterior and lateral columns adjacent to the surface (leptomeninx) of the spinal cord but not in the anterior and posterior roots. The number of GFAP-positive astrocytes increased in the anterior horn, but no such increase was observed in the white matter.

At the early symptomatic stage, *SOD1*- and ubiquitin-positive aggregates and LIs were observed in the anterior and, to a lesser extent, in the posterior horns and in the white matter of the anterior, lateral, and posterior columns. Phosphorylated neurofilament-positive spheroids were frequently observed in the posterior column as well as in the anterior and lateral columns and anterior roots; to a lesser extent, phosphorylated neurofilament-positive spheroids were observed in the posterior roots. The number of GFAP-positive astrocytes increased in the anterior horn, but no such increase was observed in the white matter.

In end-stage mice, *SOD1*- and ubiquitin-positive deposits were more predominantly observed in the white matter (as well as in the gray matter of the anterior and posterior horns) than at the early symptomatic stage (Fig. 3). Many spheroids or swollen axons showed positive immunostaining of phosphorylated neurofilaments in the anterior horns (Fig. 4) and in the anterior and posterior roots. The number of GFAP-positive astrocytes increased in the anterior horn and, to a lesser extent, in the anterior and lateral columns.

Aggregates and LIs were not immunostained for phosphorylated neurofilament (SMI-31). The spinal cord did not show any phosphorylated α-synuclein (PSer 129) or phosphorylated tau (AT8) immunoreactivity.

Electron Microscopic Findings

In mice at the early presymptomatic stage of disease (12 weeks), no definite abnormalities were detected, with the exception of tiny filamentous aggregates lacking electron-dense cores, which were only occasionally present in the neuronal processes in the anterior horns. In mice at the late presymptomatic stage (16 weeks), filamentous aggregates were not uncommonly observed in the neuronal processes, including the axons in the anterior horns. No aggregates were found in the somata or proximal dendrites of the anterior horn cells. In mice at the symptomatic stage (20 and 24 weeks), filamentous aggregates were frequently present and were predominantly found in the neuronal processes, including the proximal axons in the anterior horns. Moreover, aggregates were occasionally observed in the cytoplasm of astrocytes. The aggregates almost always consisted of interwoven intermediate filaments (~10–15 nm in diameter) that were slightly thicker than neurofilaments (Fig. 5). These aggregates were composed of loosely or compactly packed filaments and frequently contained electron-dense granular or amorphous cores at the center; as such, these aggregates with cores resembled LIs. On the other hand, the aggregates were less frequently observed in the somata or dendrites of the anterior horn neurons. Usually a single but occasionally a few aggregates were observed in the soma of a single neuron. Cord-like swollen axons with or without a myelin sheath consisted of accumulated neurofilaments running parallel to the longitudinal axis, which frequently

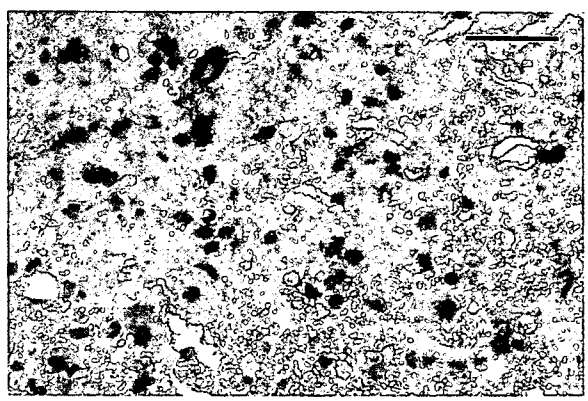

FIGURE 3. Many *SOD1*-positive deposits are observed in the gray matter of the anterior horn at the end stage (lumbar cord). Scale bar = 30 μm.

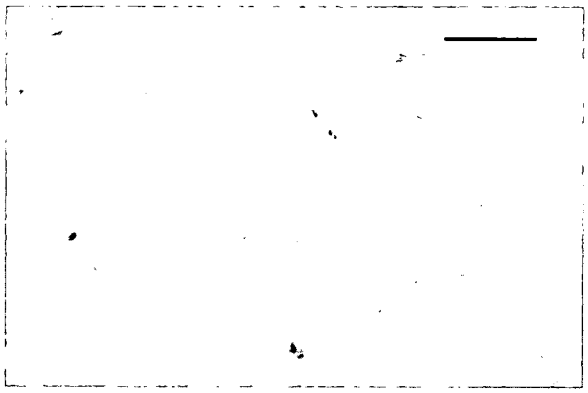

FIGURE 4. Many spheroids show positive immunostaining for phosphorylated neurofilament in the anterior horn at the end stage (lumbar cord). Scale bar = 50 μm.

contained filamentous aggregates and LIs. Vacuolated mitochondria were not found anywhere at any stage.

Immunoelectron Microscopic Findings

To determine the ultrastructural distribution of human *SOD1* and ubiquitin immunoreactivity, we used postembedding immunogold electron microscopy. A sheep polyclonal anti-human *SOD1* antibody (Calbiochem) at a dilution of 1:1000 and a polyclonal anti-ubiquitin antibody (DAKO) at a dilution of 1:500 were ideal for the detection of deposits of immunogold particles in the aggregates. Aggregates were easily identified by their characteristic structure. High levels of human *SOD1* (Fig. 6) and ubiquitin-immunogold labeling (Fig. 7) were observed in the profiles of small to large aggregates, even in samples obtained at the presymptomatic stage. Compactly packed filaments and electron-dense cores of aggregates showed more prominent *SOD1*- and ubiquitin-immunogold labeling than did loosely packed filaments. There were no significant immunogold-labeled deposits of *SOD1* or ubiquitin in the mitochondria. Phosphorylated neurofilament-immunogold labeling was not detected in the aggregates.

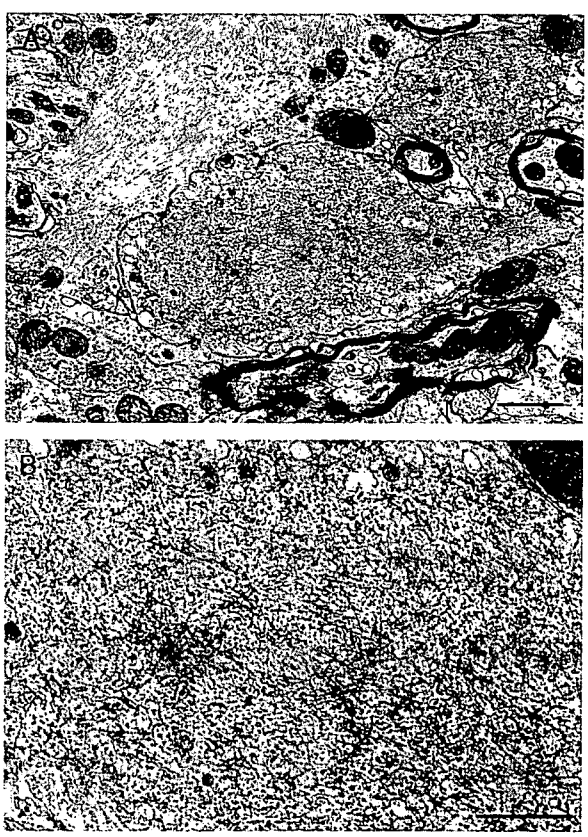

FIGURE 5. **(A)** Aggregates in the neuropil. **(B)** Higher magnification of **A**. An aggregate consists of interwoven intermediate filaments (~10–15 nm in diameter) that are slightly thicker than neurofilaments. Scale bar = 1 μm.

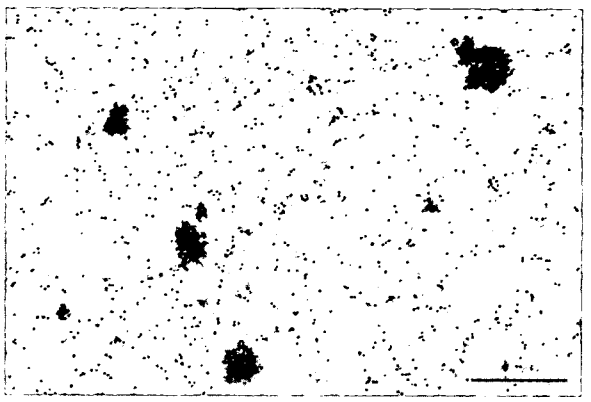

FIGURE 6. A high level of human *SOD1*-immunogold labeling is present in the aggregate. Scale bar = 1 μm.

Nontransgenic Littermates

The average number of anterior horn neurons was 14.5 ± 1.9 (n = 6). No vacuolar changes were observed. No control mice at any age showed *SOD1*- or ubiquitin-positive aggregates, LIs, or cord-like axonal swelling.

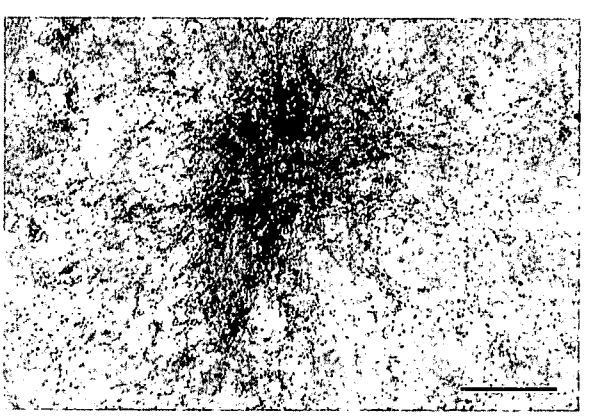

FIGURE 7. A high level of human ubiquitin-immunogold labeling is present in the aggregate. Compactly packed filaments of the aggregate show more prominent ubiquitin-immunogold labeling than loosely packed filaments. Scale bar = 1 μm.

DISCUSSION

Two main pathologic features of human mutant *SOD1* Tg mice include vacuolar formation (15–18) and the presence of *SOD1*- and ubiquitin-positive aggregates (19–22). Vacuolar formation has been identified as a dominant pathologic feature associated with motor neuron death and paralysis in mice expressing G93A or G37R mutant *SOD1* (15–18), although there remains some controversy regarding the origin and the site of vacuoles. Vacuolar pathology that at least partially represents damaged mitochondria is seen in the motor neurons of mice or rats expressing high levels of *SOD1* G93A (23–25) and *SOD1* G37R (26), but it is not seen in diseases associated with other mutations (8, 27). Mice expressing high gene copy numbers of human *SOD1* carrying the G93A mutation developed a disease with a relatively short course and with a pathology primarily characterized by severe vacuolar changes in the anterior horn neurons and their processes (23). On the other hand, G93A mutant *SOD1* Tg mice with a low transgene copy number showed no vacuoles (28). Vacuolar changes are also less apparent in affected H46R rats (8). The present study of H46R mutant *SOD1* Tg mice has revealed an initial development of muscle weakness and atrophy in the hindlimbs, as well as an absence of vacuolar formation anywhere at any stage of the disease; these features are compatible with the clinical and pathologic manifestations of patients with FALS who have an H46R mutant *SOD1* gene (4–6). Our findings suggest that vacuolar formation may not play a critical role in the pathogenesis in H46R mutant *SOD1* Tg mice or patients with an H46R mutant *SOD1* gene.

On the other hand, a feature common to all examples of *SOD1* mutant-mediated disease in mice is prominent *SOD1*-and ubiquitin-positive aggregates. *SOD1*-positive aggregates have been implicated as a potential mechanism in the pathogenesis of mutant *SOD1* Tg mice (19–22), although discrepancies have been reported in terms of both the location and distribution of aggregates. H46R rats have an abundance of aggregates, particularly late in the course of disease (8). This is the first report to demonstrate the fine structure of aggregates in H46R mutant *SOD1* Tg mice, in which *SOD1*- and ubiquitin-positive aggregates were observed as diffusely and prominently present at quite an early phase of the presymptomatic stage, primarily in the anterior horns and, to a lesser extent, in the posterior horns and the white matter, including the anterior and posterior columns; in addition, this study showed marked increases in the size and frequency of these aggregates with disease progression. Another novel finding of the present study was the electron microscopic detection of tiny aggregates in the neuropil of the anterior horn, even at the early presymptomatic stage of disease. The present results, taken together with those of preceding reports, suggest that such aggregates are characteristic of *SOD1* mutant mice and rats, although the particular site and distribution of aggregates differ somewhat among reports. Thus, it is likely that such aggregates are involved in the pathomechanism of motor neuron degeneration, although it remains unclear whether or not they play a neurotoxic or neuroprotective role.

Previous reports of other mutant *SOD1* Tg mice have noted pathologic changes that are relatively restricted to the anterior horns of the spinal cord (15, 26, 28, 29): in the spinal cord of G86R *SOD1* Tg mice, there is no significant reduction in the number of total neurons, motor neurons, or interneurons in the ventral spinal cord of presymptomatic mice (29); in the intermediate and late stages of degeneration in the spinal cord of G37R *SOD1* Tg mice, there is no degeneration of the ventral, lateral, or dorsal columns, and even at more advanced stages there is no evidence of axonal degeneration in the corticospinal tract of the dorsal column (26). In the spinal cord of G93A *SOD1* Tg mice that highly express the mutated gene (the G1 line), the main changes observed are primarily limited to the neuronal cell body; the white matter of the anterior, lateral, and posterior columns remains essentially normal at the presymptomatic and early symptomatic stages, whereas at the symptomatic stage, changes in the white matter (axonal degeneration) are localized in the anterior and lateral columns (15). On the other hand, in the spinal cord of G93A *SOD1* Tg mice, a line of low expressors of the mutated gene (G5/G5), the white matter of the anterior, lateral, and the intermediate zone of the posterior columns shows abnormalities after 200 days of age (i.e. clinical signs develop after 300 days of age), whereas the posterior roots are essentially normal, even at the symptomatic stage (28). It was thus a novel finding of the present study that in the spinal cord of H46R Tg mice, axonal degeneration extended beyond the motor system to the entire white matter, including the pyramidal tract of the posterior column and the anterior and posterior roots, as detected on Epon-embedded plastic sections by toluidine blue staining. These neuropathologic changes are mostly consistent with those of H46R rats (8); namely, in H46R rats at the presymptomatic stage, an increased number of reactive astrocytes and a reduction in the number of large anterior horn neurons are observed, together with an increase in the number of microglia in the anterior horn; ubiquitination of the dendrites and axons are evident in the anterior horn of the lumbar spinal cord, and at the symptomatic stage there is a marked loss of large motor neurons as well as site of swelling in the axons in the anterior horn (8). However, there is no description of the involvement of the white matter, anterior roots, or posterior roots in H46R rats. Aggregates and LIs are observed after the onset of clinical signs in H46R rats, whereas H46R mice already show such signs, primarily in the anterior horns, even at the presymptomatic stage. In this study, the ultrastructures of the aggregates and LIs, both of which consisted of interwoven intermediate filaments, showed deposits of ubiquitin- and *SOD1*-immunogold labeling; these results are consistent with those described in previous reports on other mutant *SOD1* Tg mice such as G93A mice (22).

In autopsy cases of patients FALS who had an H46R mutation in the *SOD1* gene, *SOD1*- and ubiquitin-positive aggregates and inclusions are not present in the spinal cord, including the neuropil and the remaining anterior horn cells (5, 6). This feature stands in contrast to the presence of LIs in H46R mutant *SOD1* Tg mice; the difference is probably

due to a longstanding course in affected humans with a severe depletion of anterior horn neurons. Moreover, in 1 of 2 autopsy reports, the corticospinal tracts, posterior column, and anterior and posterior spinocerebellar tracts were found to be degenerated (5), whereas in the other report, the lateral columns, including the spinocerebellar tracts and the anterior funiculi, were atrophic, although the posterior column was preserved (6). These previous findings are consistent with the present findings obtained with H46R mutant *SOD1* Tg mice in that the degenerative changes extend over the entire white matter (including the anterior, lateral, and posterior columns) with time.

Thus, the H46R *SOD1* mutation is clinically characterized as a "pseudopolyneuritic form of ALS" with lower motor neuron-dominant involvement developing in the lower extremities and a markedly longstanding clinical course, and pathologic, widespread changes extending beyond the motor system to the entire white matter, and the anterior and posterior roots; in this line of mutant mice, these features are accompanied by numerous *SOD1*- and ubiquitin-positive aggregates lacking vacuoles. This animal model of H46R mutant *SOD1* Tg mice is suitable for the investigation of human FALS with an H46R mutant *SOD1* gene because of the close pathologic similarity between the 2 diseases. Further examination is needed to locate the site at which the aggregates predominate and originate (e.g. in the somata of the anterior horn neurons, dendrites, axons, or non-neuronal cells [astrocytes and microglia]). It will also be necessary to elucidate whether these aggregates are neurotoxic and thereby involved in the pathomechanism in these Tg mice or whether they are only a bystander and instead exert some neuroprotective function.

REFERENCES

1. Gaudette M, Hirano M, Siddique T. Current status of *SOD1* mutations in familial amyotrophic lateral sclerosis. Amyotroph Lateral Scler Other Motor Neuron Disord 2000;1:83–89
2. Gurney ME. Transgenic-mouse model of amyotrophic lateral sclerosis. N Engl J Med 1994;331:1721–22
3. Ripps ME, Huntley GW, Hof PR, Morrison JH, Gordon JW. Transgenic mice expressing an altered murine superoxide dismutase gene provide an animal model of amyotrophic lateral sclerosis. Proc Natl Acad Sci U S A 1995;92:689–93
4. Aoki M, Ogasawara M, Matsubara Y, et al. Familial amyotrophic lateral sclerosis (ALS) in Japan associated with H46R mutation in Cu/Zn superoxide dismutase gene: A possible new subtype of familial ALS. J Neurol Sci 1994;126:77–83
5. Ohi T, Saita K, Takechi S, et al. Clinical features and neuropathological findings of familial amyotrophic lateral sclerosis with a His 46Arg mutation in Cu/Zn superoxide dismutase. J Neurol Sci 2002;197:73–78
6. Arisato T, Okubo R, Arata H, et al. Clinical and pathological studies of familial amyotrophic lateral sclerosis (FALS) with *SOD1* H46R mutation in large Japanese families. Acta Neuropathol (Berl) 2003; 106:561–68
7. Patrikios JS. Contribution à l'Étude des Formes Cliniques et de l'Anatomie Pathologique de la Sclérose Latérale Amyotrophique. Thèse, Paris University, Paris, 1918
8. Nagai M, Aoki M, Miyoshi I, et al. Rats expressing human cytosolic copper-zinc superoxide dismutase transgenes with amyotrophic lateral sclerosis: Associated mutations develop motor neuron disease. J Neurosci 2001;21:9246–54
9. Ioannou PA, Amemiya CT, Garnes J, et al. A new bacteriophage P1-derived vector for the propagation of large human DNA fragments. Nat Genet 1994;6:84–89
10. Levanon D, Lieman-Hurwitz J, Dafni N, et al. Architecture and anatomy of the chromosomal locus in human chromosome 21 encoding the Cu/Zn superoxide dismutase. EMBO J 1985;4:77–84
11. Elroy-Stein O, Bernstein Y, Groner Y. Overproduction of human Cu/Zn-superoxide dismutase in transfected cells: Extenuation of paraquat-mediated cytotoxicity and enhancement of lipid peroxidation. EMBO J 1986;5:615–22
12. Hashimoto-Gotoh T, Mizuno T, Ogasahara Y, et al. An oligodeoxyribonucleotide-directed dual amber method for site-directed dual amber method for site-directed mutagenesis. Gene 1995;152:271–75
13. Beauchamp C, Fridovich I. Superoxide dismutase: Improved assays and an assay applicable to acrylamide gels. Anal Biochem 1971:44:276–87
14. Iwatsubo T. Aggregation of α-synuclein in the pathogenesis of Parkinson's disease. J Neurol 2003;250(Suppl 3):III/11–III/14
15. Dal Canto MC, Gurney ME. Neuropathological changes in two lines of mice carrying a transgene for mutant human Cu,Zn *SOD*, and in mice overexpressing wild-type human *SOD*: A model of familial amyotrophic lateral sclerosis (FALS). Brain Res 1995;676:25–40
16. Wong PC, Pardo CA, Borchelt DR, et al. An adverse property of a familial ALS-liked *SOD1* mutation causes motor neuron disease characterized by vacuolar degeneration of mitochondria. Neuron 1995; 14:1105–16
17. Kong J, Xu Z. Massive mitochondrial degeneration in motor neurons triggers the onset of amyotrophic lateral sclerosis in mice expressing a mutant *SOD1*. J Neurosci 1998;18:3241–50
18. Sasaki S, Warita H, Murakami T, Abe K, Iwata M. Ultrastructural study of mitochondria in the spinal cord of transgenic mice with a G93A mutant *SOD1* gene. Acta Neuropathol (Berl) 2004;107:461–74
19. Beaulieu JM, Jacomy H, Julien JP. Formation of intermediate filament protein aggregates with disparate effects in two transgenic mouse models lacking the neurofilament light subunit. J Neurosci 2000;20: 5321–28
20. Bruijin LI, Houseweart MK, Kato S, et al. Aggregation and motor neuron toxicity of an ALS-linked *SOD1* mutant independent from wild-type *SOD1*. Science 1998;281:1851–54
21. Johnston JA, Dalton MJ, Gurney ME, Kopito RR. Formation of high molecular weight complexes of mutant Cu,Zn-superoxide dismutase in a mouse model for familial amyotrophic lateral sclerosis. Proc Natl Acad Sci U S A 2000;97:12571–76
22. Sasaki S, Warita H, Murakami T, et al. Ultrastructural study of aggregates in the spinal cord of transgenic mice with a G93A mutant *SOD1* gene. Acta Neuropathol (Berl) 2005;109:247–55
23. Dal Canto MC, Gurney ME. Development of central nervous system pathology in a murine transgenic model of human amyotrophic lateral sclerosis. Am J Pathol 1994;145:1271–79
24. Jaarsma D, Rognoni F, van Duijn W, Verspaget HW, Haasdijk ED, Holstege JC. CuZn superoxide dismutase (*SOD1*) accumulates in vacuolated mitochondria in transgenic mice expressing amyotrophic lateral sclerosis-linked *SOD1* mutations. Acta Neuropathol (Berl) 2001; 102:293–305
25. Sasaki S, Warita H, Murakami T, Abe K, Iwata M. Ultrastructural study of mitochondria in the spinal cord of transgenic mice with a G93A mutant *SOD1* gene. Acta Neuropathol (Berl) 2004;107:461–74
26. Wong PC, Pardo CA, Borchelt DR, et al. An adverse property of a familial-ALS linked *SOD1* mutation causes motor neuron disease characterized by vacuolar degeneration of mitochondria. Neuron 1995; 14:1105–16
27. Bruijn LI, Becher MW, Lee MK, et al. ALS-linked *SOD1* mutant G85R mediates damage to astrocytes and promotes rapidly progressive disease with *SOD1*-containing inclusions. Neuron 1997;18:327–38
28. Dal Canto MC, Gurney ME. A low expressor line of transgenic mice carrying a mutant human Cu,Zn superoxide dismutase (*SOD1*) gene develops pathological changes that most closely resemble those in human amyotrophic lateral sclerosis. Acta Neuropathol (Berl) 1997;93: 537–50
29. Morrison BM, Janssen WG, Gordon JW, Morrison JH. Time course of neuropathology in the spinal cord of G86R superoxide dismutase transgenic mice. J Comp Neurol 1998;391:64–77

An *In Vitro* Model for Lewy Body-Like Hyaline Inclusion/ Astrocytic Hyaline Inclusion: Induction by ER Stress with an ALS-Linked SOD1 Mutation

Satoru Yamagishi[1,2*☯¤a], Yoshihisa Koyama[1,2☯], Taiichi Katayama[1,2☯¤b], Manabu Taniguchi[1,2], Junichi Hitomi[1,2], Masaaki Kato[3], Masashi Aoki[3], Yasuto Itoyama[3], Shinsuke Kato[4*], Masaya Tohyama[1,2]

1 Department of Anatomy and Neuroscience, Graduate School of Medicine, Osaka University, Suita, Osaka, Japan, 2 The 21st Century Center of Excellence Program, Graduate School of Medicine, Osaka University, Suita, Osaka, Japan, 3 Department of Neurology, Tohoku University School of Medicine, Sendai, Japan, 4 Department of Neuropathology, Institute of Neurological Sciences, Faculty of Medicine, Tottori University, Yonago, Japan

Neuronal Lewy body-like hyaline inclusions (LBHI) and astrocytic hyaline inclusions (Ast-HI) containing mutant Cu/Zn superoxide dismutase 1 (SOD1) are morphological hallmarks of familial amyotrophic lateral sclerosis (FALS) associated with mutant SOD1. However, the mechanisms by which mutant SOD1 contributes to formation of LBHI/Ast-HI in FALS remain poorly defined. Here, we report induction of LBHI/Ast-HI-like hyaline inclusions (LHIs) *in vitro* by ER stress in neuroblastoma cells. These LHI closely resemble LBHI/Ast-HI in patients with SOD1-linked FALS. LHI and LBHI/Ast-HI share the following features: 1) eosinophilic staining with a pale core, 2) SOD1, ubiquitin and ER resident protein (KDEL) positivity and 3) the presence of approximately 15–25 nm granule-coated fibrils, which are morphological hallmark of mutant SOD1-linked FALS. Moreover, in spinal cord neurons of L84V SOD1 transgenic mice at presymptomatic stage, we observed aberrant aggregation of ER and numerous free ribosomes associated with abnormal inclusion-like structures, presumably early stage neuronal LBHI. We conclude that the LBHI/Ast-HI seen in human patients with mutant SOD1-linked FALS may arise from ER dysfunction.

Citation: Yamagishi S, Koyama Y, Katayama T, Taniguchi M, Hitomi J, et al (2007) An *In Vitro* Model for Lewy Body-Like Hyaline Inclusion/Astrocytic Hyaline Inclusion: Induction by ER Stress with an ALS-Linked SOD1 Mutation. PLoS ONE 2(10): e1030. doi:10.1371/journal.pone.0001030

INTRODUCTION

Amyotrophic lateral sclerosis (ALS) is a progressive neurodegenerative disorder in which both upper and lower motor neurons begin to degenerate in middle-aged persons. About 10% of ALS patients demonstrate autosomal dominant inheritance of this disease, a disorder known as familial ALS (FALS) [1–6]. About 20% of FALS cases are associated with mutations of the Cu/Zn-superoxide dismutase (SOD1) gene [7]. SOD1 is an abundant protein of approximately 153 amino acids that accounts for approximately 1% of total cytosolic protein. More than 100 different SOD1 mutations have been reported as risk factors in association with FALS.

The endoplasmic reticulum (ER) is responsible for the synthesis, initial post-translational modification, and proper folding of proteins, as well as for their sorting export and delivery to appropriate cellular destinations. A variety of conditions, such as loss of the intraluminal oxidative environment or loss of calcium homeostasis, can cause accumulation of misfolded proteins in the ER. To cope with such accumulation, there are three possible responses in eukaryotes. The first response is known as the unfolded protein response (UPR), in which IRE1α and ATF6 recognize aberrant proteins and increase the expression of ER-resident chaperones such as GRP78/BiP and GRP94 to promote proper protein folding [8,9]. The second response involves suppression of translation mediated by the serine/threonine kinase PERK, which phosphorylates and inactivates the translation initiation factor eIF-2α to reduce the production of misfolded proteins [10,11]. The third response is ER-associated degradation (ERAD), in which misfolded proteins are expelled from the ER and targeted for degradation by cytoplasmic proteasomes [12,13]. Although these three protective responses can transiently control the accumulation of misfolded proteins within the ER, they can be overcome by sustained 'ER stress' [14–16]. 'ER stress' is involved in neuronal death and various neurodegenerative disorders, such as Charcot-Marie-Tooth disease, and is especially related to inclusion body diseases such as Alzheimer's disease, Parkinson's disease, Huntington's disease and ALS [17–23].

Histopathologic studies have revealed that neuronal Lewy body-like hyaline inclusions (LBHI) and astrocytic hyaline inclusions (Ast-HI), are morphological hallmarks of mutant SOD1-linked FALS [24]. Neuronal LBHI and Ast-HI are ultrastructually identical and share various features, with both consisting of 15–25 nm granule-coated fibrils, both showing immunoreactivity for

Academic Editor: Xiao-Jiang Li, Emory University, United States of America

Received February 28, 2007; **Accepted** September 23, 2007; **Published** October 10, 2007

Funding: This work was supported in part by a grant from the 21st Century COE Program, Japan Society for the Promotion of Science, 6 Ichibancho, Chiyoda-ku, Tokyo 102-8471, Japan, a Grant-in-Aid for Scientific Research (c) from the Ministry of Education, Culture, Sports, Science and Technology of Japan (S.K.: 17500229), a Grant from Research on Psychiatric and Neurological Disease and Mental Health (SK, MA, YI) and a Research Grant on Measures for Intractable Diseases from the Ministry of Health, Labour and Welfare of Japan (SK, YI). SY is supported by a long-term fellowship by European Molecular Biology Organization (EMBO) and Japan Society for the Promotion of Science (JSPS).

Competing Interests: The authors have declared that no competing interests exist.

* **To whom correspondence should be addressed.** E-mail: yamagishi@neuro.mpg.de (SY); kato@grape.med.tottori-u.ac.jp (SK)

☯ These authors contributed equally to this work.

¤a **Current address:** Molecular Neurobiology, Max-Planck-Institute of Neurobiology, Martinsried, Munich, Germany,
¤b **Current address:** Department of Anatomy and Neuroscience, Hamamatsu University School of Medicine, Hamamatsu, Shizuoka, Japan

SOD1, ubiquitin, and copper chaperone for SOD (CCS), and both appearing late in the course of the disease (i.e. at ~10 to 30 years of age in humans [24–27]). Recently, Wate et al. reported that neuronal LBHI are immunoreactive for GRP78/BiP, a component of the UPR cellular response to ER stress [28].

In the present study, we show that ER stress in a neuroblastoma line expressing mutant SOD1 can provoke SOD1 aggregation in ER and formation of LBHI/Ast-HI-like hyaline inclusion bodies (LHIs), which show SOD1, ubiquitin, GRP78/BiP and ER resident protein (KDEL) immunopositivity similar to the shared cytopathological features of LBHI and Ast-HI. Induced neuroblastoma LHI furthermore consisted of 15–25 nm granule-coated fibrils, a hallmark of mutant SOD1-linked FALS, raising the possibility that these acutely induced aggregations represent a precursor to LBHI/Ast-HI seen in advanced FALS. In support of this possibility, we observe abnormal ER and numerous free ribosomes aggregated in the peri-nuclear region neuroblastoma cells expressing L84V SOD1 under ER stress condition and in spinal cord neurons in presymptomatic transgenic mice expressing L84V SOD1. Taken together, these findings suggest a model for early events in FALS cellular pathology, in which ER stress promotes the aggregation of mutant SOD1 and is involved in the development of LBHI/Ast-HI in patients with mutant SOD1 linked FALS.

RESULT

Aggregation and ubiquitination of mutant SOD1 under ER stress

To identify conditions which lead to the aggregation of mutant SOD1, we generated SK-N-SH human neuroblastoma cell lines that stably expressed FLAG-tagged human SOD1 encoding a leucine to valine substitution mutation (L84V) associated with FALS [29]. Western blot analysis confirmed that expression of endogenous and exogenous SOD1 was equal in the cell line (Fig. 1A). Reports that neuronal LBHI contain GRP78/BiP, an ER resident component of the UPR response, suggested that ER stress might be a factor in the aggregation of mutant SOD1 [28]. We therefore examined localization of wild-type and mutant SOD1 under normal conditions and under conditions of ER stress (Figure 1). Under normal conditions, wild-type and L84V SOD1 were distributed through the cytosol (Fig. 1B and D). However, following treatment with tunicamycin, an inhibitor of N-glycosylation which causes ER stress, small SOD1-positive aggregates (up to 3 μm in diameter) were seen in L84V SOD1-expressing cells (22.3%, $p<0.001$; Fig. 1E and F). A much smaller percentage of wild-type SOD1 expressing cells (2.9%, n.s.) showed non-inducible SOD1 aggregation (Fig. 1C and F). To confirm whether ER stress is required for the aggregation of SOD1, we compared tunicamycin and thapsigargin as ER stress inducers with etoposide as a non-ER stress inducer (causing DNA damage). Exposure to 1 and 3 μg/ml tunicamycin (21.1% and 17.5%, respectively) or 0.3 and 1 μM thapsigargin (27.0% and 27.2%, respectively) significantly increased the number of cells containing SOD1 aggregates, in L84V SOD1 expressing neuroblastoma cells. Treatment with 100 and 300 μM etoposide did not lead to a significant increase in aggregates (Fig. 1G). Thus mutant SOD1 forms aggregates following treatments provoking ER stress, but not following treatment causing damage to the nucleus.

Since the SOD1-positive inclusions of FALS patients are known to be eosinophilic [26], we performed hematoxylin-eosin (HE) and anti-SOD1 antibody staining to determine whether the aggregates induced in the neuroblastoma line were also eosinophilic.

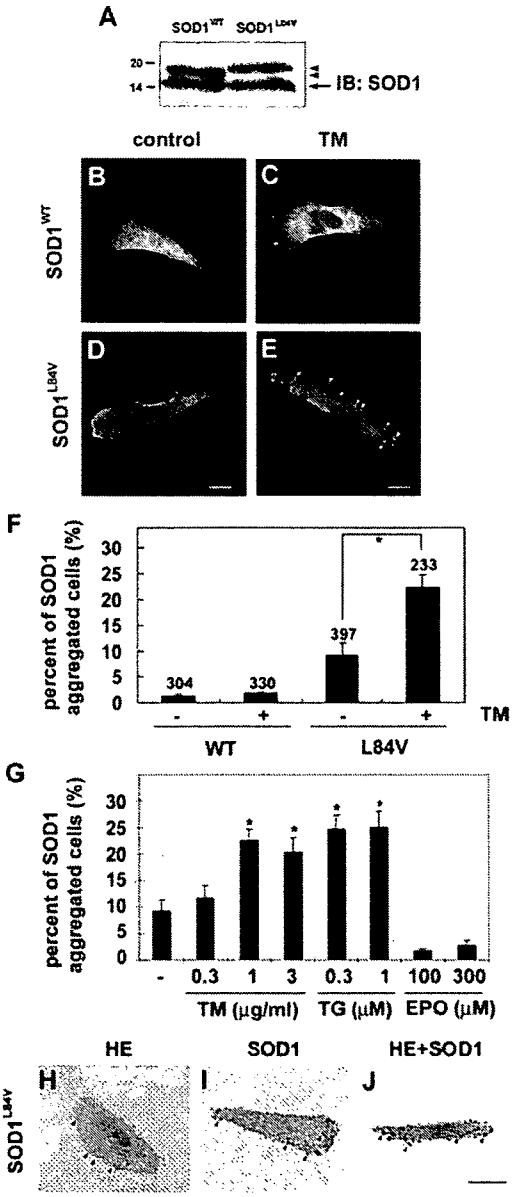

Figure 1. Eosinophilic aggregates of L84V SOD1 are induced by ER stress. (A) Western blotting analysis of the expression of SOD1 in SK-N-SH cells, which stably expressed FLAG tagged wild-type SOD1 or L84V mutant SOD1. Arrowheads and arrow indicate exogenous and endogenous SOD1, respectively. (B–D) Immunofluorescent analysis of SOD1 aggregates in SK-N-SH cells expressing wild-type SOD1 (B, C) or L84V SOD1 (D, E). Cells were incubated under control conditions (B, D) or with 1 μg/ml tunicamycin (C, E) for 24 h, and then were fixed and stained with an anti-SOD1 antibody. Tunicamycin induced aggregates of SOD1 (arrowheads) in L84V SOD1-expressing cells, but not in wild-type SOD1-expressing cells. Scale bar = 20 μm. (F) Quantification of (B-D). After the staining the cells with SOD1 aggregates were counted and scored. Numbers indicate the amounts of total counted cells. Asterisks show a significant difference from control, *$p<0.001$. (G) SOD1 aggregates induced by tunicamycin and thapsigargin, but not by etoposide. SK-N-SH cells expressing L84V SOD1 were exposed to 0.3, 1 and 3 μg/ml tunicamycin, 0.3 and 1 μM thapsigargin and 100 and 300 μM etoposide. Asterisks show a significant difference from control, *$p<0.001$. (H-J) Eosinophilic SOD1 aggregates induced by tunicamycin. Cells were treated as described in (E) and then stained with HE (H), anti-SOD1 antibody (I), or both (J). Scale bar = 20 μm.
doi:10.1371/journal.pone.0001030.g001

Figures 1H-J show that the aggregates induced by tunicamycin treatment were positive for both eosin and SOD1.

In patients with mutant SOD1-linked FALS, SOD1-positive aggregates are reported to be ubiquitinated by RING finger-type E3 ubiquitin ligases such as dorfin [30–33]. To investigate whether the SOD1 aggregates induced by ER stress were ubiquitinated, we performed double immunostaining with anti-SOD1 and anti-ubiquitin antibodies (Fig. 2 A–R). After treatment with either tunicamycin or ALLN, a specific proteasome inhibitor, wild-type and L84V SOD1-expressing cells were immunostained with anti-SOD1 and anti-ubiquitin antibodies. As a result, mutant SOD1 aggregates induced by either tunicamycin or ALLN were clearly colocalized with ubiquitin, suggesting the SOD1 were ubiquitinated. To further examine the ubiquitination of the mutant SOD1, a co-immunoprecipitation assay utilizing ubiquitin was performed (Fig. 2S). As expected, L84V SOD1-expressing cells showed a positive ubiquitin ladder after ALLN treatment, but wild-type SOD1-expressing cells did not.

Aggregates of SOD1 show positive localization to the ER, but not to the mitochondria, lysosomes, or Golgi apparatus

Under normal conditions, SOD1 is diffusely distributed throughout the cytoplasm. In contrast, under the pathological condition, SOD1 aggregates are associated with specific organelles such as the mitochondria and/or ER [34–37]. Since the tunicamycin-induced aggregates of mutant SOD1 were localized to the central and peripheral regions of the cytoplasm (Fig. 1E, H–J), we investigated the subcellular localization of these aggregates with organelle specific markers. Confocal microscopy analysis clearly showed colocalization of SOD1 and an ER retention signal

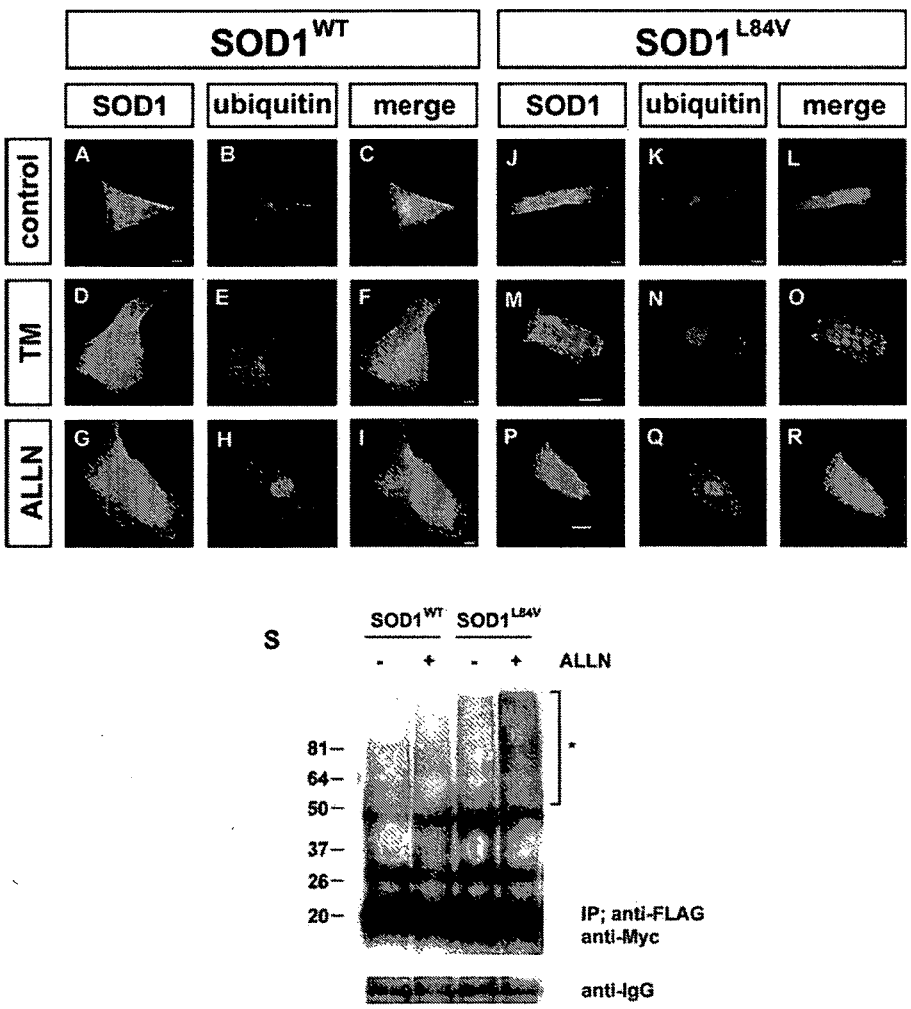

Figure 2. Ubiquitination of mutant SOD1 aggregates. (**A–R**) Colocalization assay with SOD1 and ubiquitin. SK-N-SH cells expressing wild-type SOD1 (**A–I**) or L84V SOD1 (**J–R**) were incubated with 1 μg/ml of tunicamycin (**D–F, M–O**), 4 μg/ml of ALLN (**G–I, P–R**), or no agents (**A–C, J–L**) for 24 h. Then the cells were fixed and stained with anti-SOD1 antibody (green; **A, D, G, J, M, P**) or anti-ubiquitin antibody (red; **B, E, H, K, N, Q**). Arrows indicate colocalization of SOD1 aggregates and ubiquitin. Scale bar = 20 μm. (**S**) Co-immunoprecipitation assay utilizing ubiquitin. SK-N-SH cells stably expressing wild-type and L84V SOD1 were transfected with a myc-tagged ubiquitin expression vector. After incubation with or without ALLN, cell lysates were prepared and assayed with anti-myc antibody of the immunoprecipitant with anti-FLAG antibody. Asterisk shows an ubiquitinated ladder that appeared after ALLN treatment of L84V SOD1-expressing cells. IgG bands are shown as loading controls.
doi:10.1371/journal.pone.0001030.g002

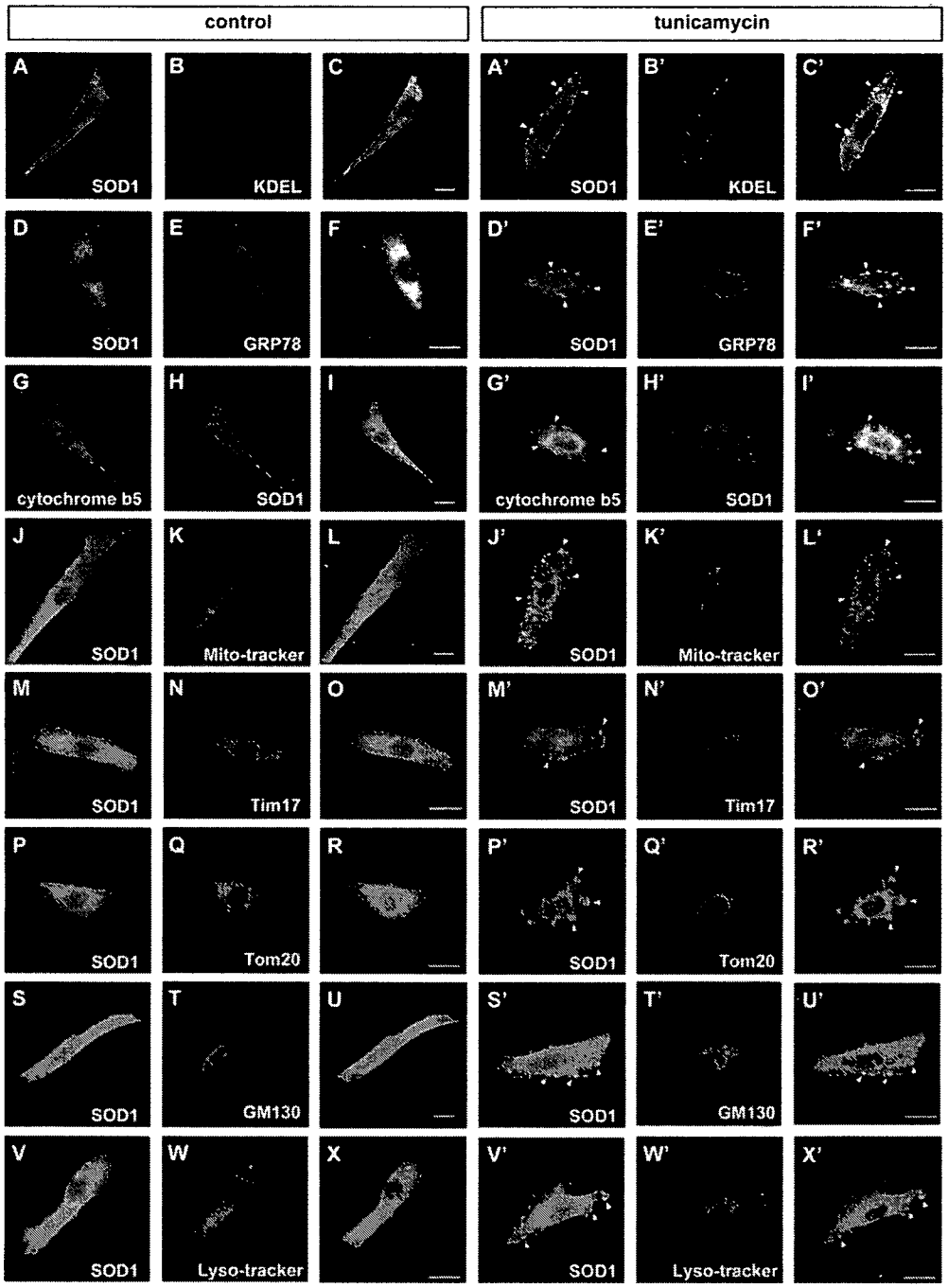

Figure 3. Positive translocation of SOD1 aggregates to ER, but not to the mitochondria, Golgi apparatus, or lysosomes. (**A–I, A'–I'**) Stress-dependent localization of SOD1 to the ER. L84V SOD1-expressing SK-N-SH cells were incubated for 24 h without (**A–I**) or with 1 μg/ml of tunicamycin (**A'–I'**). Then the cells were fixed and stained using an anti-SOD1 antibody (green; **A, D, A', D'**) and an anti-KDEL antibody (red; **B, B'**) or an anti-GRP78/BiP antibody (red; **E, E'**). GFP-cytochrome b5 were transfected to the cells and stained with anti-GFP (green; **G, G'**) and anti-SOD1 (red; **H, H'**) antibodies. Merged images (**C, F, I, C' F', I'**). The aggregates of SOD1 (arrowheads) are positive for KDEL, GRP78/BiP and cytochrome b5. (**J–R, J'–R'**) Analysis of SOD1 localization to the mitochondria. L84V SOD1-expressing SK-N-SH cells were treated as described in above. The locations of the mitochondria and SOD1 were visualized in L84V SOD1-expressing SK-N-SH cells using 100 nM Mito-tracker (red; **K, K'**), an anti-Tim17 antibody (red; N, N') or an anti-Tom20 antibody (red; **Q, Q'**) and an anti-SOD1 antibody (green; **J, M, P, J', M', P'**). Merged images (**L, O, R, L', O', R'**). (**S–U, S'–U'**) Investigation of SOD1 localization to the Golgi apparatus. L84V SOD1-expressing SK-N-SH cells were treated as described in above. Then the cells were stained with anti-SOD1 antibody (green; **S, S'**) and anti-GM130 antibody (red; **T, T'**). Merged images (**U, U'**). (**V-X, V'-X'**) Analysis of the localization of SOD1 to the lysosomes. A GFP-tagged L84V SOD1 vector was transfected into L84V SOD1-expressing SK-N-SH cells. After 24 h of incubation with 1 μg/ml of tunicamycin, the cells were incubated for a further 30 min with 100 nM Lyso-tracker (red; **W, W'**) to visualize the lysosomes. GFP channel (**V, V'**) Merged images (**X, X'**). Scale bars = 20 μm. Arrowheads indicate aggregated SOD1.
doi:10.1371/journal.pone.0001030.g003

(KDEL) containing protein and GRP78/BiP, suggesting SOD1 localization in ER (Fig. 3A–F, A′–F′). In order to confirm the SOD1 colocalization with ER, we utilized GFP conjugated cytochrome b5, a typical C-terminal anchored ER membrane protein. As expected, SOD1 showed the positive staining with cytochrome b5, indicating mutant SOD1 localization to ER (Fig. 3G–I, G′–I′). In the absence of stress, ER was located to the perinuclear region. However, treatment with tunicamycin seemed to cause its relocation to an abnormal region near the cell periphery. The aberrant distribution of ER following tunicamycin treatment was not observed in cells expressing wild type SOD1 (Fig. S1C′, F′ and I′). These results suggest deterioration of ER function and localization due to aggregation of mutant SOD1.

In light of previous reports identifying mutant SOD1 colocalization to the mitochondria [34,35,37], we also examined the potential colocalization of mutant SOD1 with mitochondria. In contrast to the results with markers for ER, the SOD1 aggregates induced by tunicamycin did not colocalize with the mitochondria marker Mitotracker, with Tim17 which marks the mitochondrial inner membrane nor Tom20 which marks the mitochondrial outer membrane (Fig. 3J′–R′). The localization of these SOD1 aggregates also did not correspond with the Golgi apparatus or the lysosomes, which were stained by anti-GM130 antibody and Lyso-tracker, respectively (Fig. 3S′–X′).

Our previous results in figure 3C′, F′ and I′ revealed aberrant redistribution of ER membranes in tunicamycin-treated mutant SOD1 expressing cells to the cell periphery region. To directly visualize the localization of ER, we performed electron microscopic analysis of tunicamycin-stressed cells expressing mutant SOD1. Figure 4A and B showed abnormal aggregates of rough ER, sac-like structures with surface ribosomes, associated with numerous free ribosomes. Mutant SOD1 localization to these peripheral aggregates was confirmed by immunoelectron microscopy (Fig. 4C), implying defective functional activities of ER and free ribosomes in cells expressing mutant SOD1.

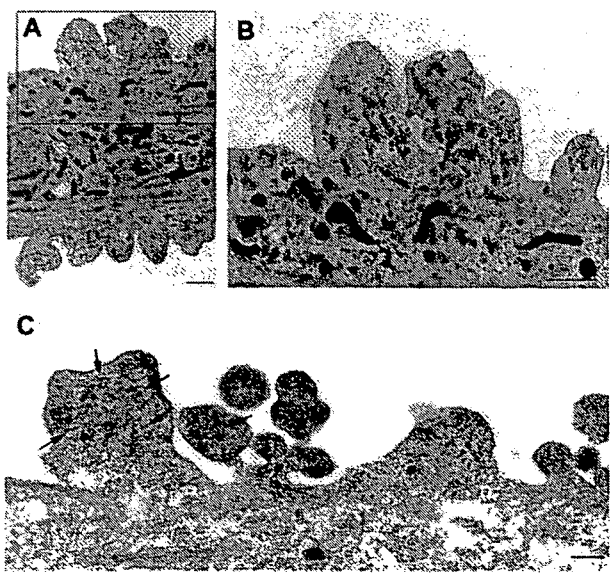

Figure 4. ER and SOD1 co-localization in peri-cytoplasmic membrane region. (**A**) Electron micrograph of L84V SOD1-expressing SK-N-SH cells after treatment with 1 μg/ml of tunicamycin for 24 h as described in Materials and Methods. (**B**) Enlargement of part of (**A**). Arrowheads indicate abnormal ER aggregates, where mutant SOD1 is localized as in Fig. 3C′ and 3E′. Scale bar = 1 μm. (**C**) SOD1 localization in peri-cytoplasmic membrane region. Cells were treated as described in (**A**) and immune electron micrograph was obtained as described in Materials and Methods. Arrows show SOD1 immunoreactive in ER.
doi:10.1371/journal.pone.0001030.g004

LBHI/Ast-HI-like Inclusions are induced by ER stress.

Wate et al. [28] reported that neuronal LBHI in G93A SOD1 transgenic mice are immune reactive for GRP78/BiP, an ER resident component of the UPR response. As shown in figures 3A′-I′ and 4C, mutant SOD1 localized to the ER following stress induction by tunicamycin. These SOD1 aggregates shared additional features with LBHI/Ast-HI, namely eosin positivity and ubiquitin immune reactivity. Those observations led us to consider whether ER stress would eventually induce the formation of full-fledged LBHI/Ast-HI. To test this hypothesis, we examined whether inclusion bodies containing mutant SOD1 developed in L84V SOD1-expressing cells subjected to ER stress. Consistent with this idea, eosinophilic hyaline inclusions (~10 to 20 μm in diameter) with a pale core, which are similar to neuronal LBHI/Ast-HI in the spinal cord of ALS patients harboring a SOD1 mutation, developed within 24 hrs of exposure to tunicamycin (Fig. 5A), but not in cells expressing wild type SOD1 (data not shown). In fact, the eosin-positive LBHI/Ast-HI-like hyaline inclusions (LHIs) were morphologically similar to the Ast-HI seen in the spinal cord of transgenic L84V SOD1 mice at the symptomatic stage (Fig. 5A and D). Furthermore, ultrastructual analysis revealed that the LHIs in neuroblastoma cells were composed of granule-coated fibrils (approximately 15–25 nm in diameter) and granular materials, which are the typical morpho-

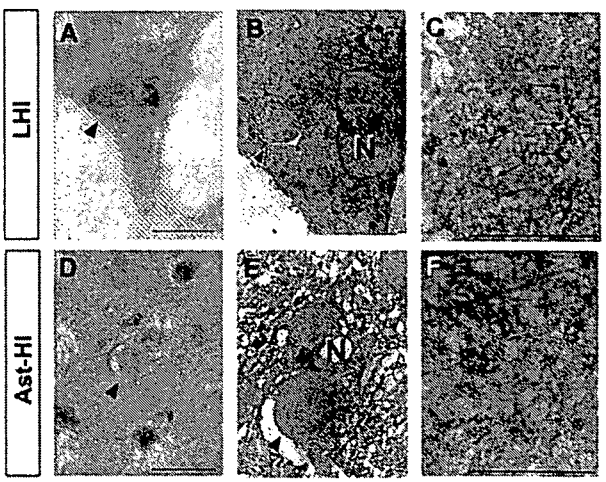

Figure 5. LHIs containing granule-coated fibrils are morphologically identical with Ast-HI from L84V transgenic mice. (**A–F**) Comparison of a LHI induced by ER stress in an L84V SOD1-expressing SK-N-SH cell (**A–C**) and Ast-HI in the spinal cord of a transgenic L84V SOD1 mouse (**D–F**). (**A**) An eosinophilic LHI in the cytoplasm of the SK-N-SH cell expressing L84V SOD1 cell was induced by treatment with 1 μg/ml of tunicamycin for 24 h (scale bar = 20 μm). (**B**) Electron micrograph of a hyaline inclusion (arrow) obtained by the direct epoxy resin-embedding method after decolorization of the HE-stained section shown in (**A**). N, nucleus; ×3000 (scale bar = 1 μm). (**C**) At a high magnification, the inclusion is composed of granule-coated fibrils (arrows) approximately 15–25 nm in diameter and granular materials. ×16000 (scale bar = 1 μm). (**D**) An eosinophilic Ast-HI from a transgenic L84V SOD1 mouse. (**E**) Electron micrograph of an Ast-HI obtained by the direct epoxy resin-embedding method mentioned in (**B**). N, nucleus; ×2000 (scale bar = 1 μm). (**F**) Enlargement of (**E**). ×16000 (scale bar = 1 μm). Note that the fibrils observed in (**C**) and (**F**) are ultrastructually identical.
doi:10.1371/journal.pone.0001030.g005

logical hallmarks of mutant SOD1-linked FALS, and were identical with the Ast-HI found in L84V SOD1 mice (Fig. 5C, F; [38]). These results suggest that LBHI/Ast-HI in FALS patients might be provoked by ER stress as we observed for LHIs.

We further explored the molecular similarity between the LHI and LBHI/Ast-HI, using double-label immunocytochemistry. As shown in figure 6A–D, LHIs induced by tunicamycin are immunopositive for anti-SOD1 and anti-ubiquitin antibodies, consistent with the LBHI/Ast-HI features. In the spinal cord of G93A SOD1 mutant mice at the symptomatic stage, neuronal LBHI show GRP78/BiP immunoreactive, suggesting the involvement of ER resident protein [28]. Therefore, we examined whether LHIs also contain ER resident protein. As expected, LHI showed anti-KDEL positivity, indicating the involvement of ER resident proteins such as calreticulin, GRP 94, PDI and GRP78/BiP in LHI development (Fig. 6E and F). Furthermore, Ast-HI in spinal cord of L84V SOD1 transgenic mice at symptomatic stage also showed KDEL positive (Fig. 6G and H), meaning that the principle features of these inclusions in neuroblastoma cells and the LBHI/Ast-HI of FALS patients are the same and implying LHI and LBHI/Ast-HI might develop in similar procedure.

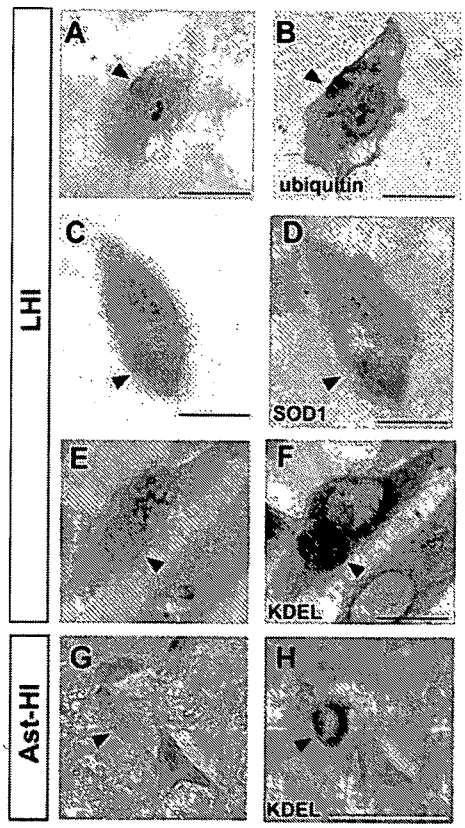

Figure 6. Positive immunoreactive against ubiquitin, SOD1 and KDEL of LHIs. (A–D) LHIs show immunoreactive against ubiquitin and SOD1. Eosinophilic LHIs in SK-N-SH cells (arrowheads in A and C) induced by tunicamycin were immunostained for ubiquitin (B) and SOD1 (D) after de-colorization. (E–H) KDEL immunoreactive in both LHI and Ast-HI. Eosinophilic LHI in SK-N-SH cells (arrowhead in E) and Ast-HI in spinal cord of L84V SOD1 mouse (arrowhead in G) were immunostained against anti-KDEL antibody after de-colorization (F, H). Scale bar = 20 μm

doi:10.1371/journal.pone.0001030.g006

Abnormal ER aggregated around peri-nuclear region with numerous free ribosomes at presymptomatic stage of Ast-HI in L84V SOD1 mice.

To further explore the relationship of LHI to the development of LBHI/Ast-HI in FALS patients with mutant SOD1, we performed ultrastructual examination of transgenic L84V SOD1 mice, which show neuronal LBHI and Ast-HI at symptomatic stage (Fig. 5D–F, 6G–H; [35]). We examined the mice at the presymptomatic stage in the hope of detecting precursors to hyaline inclusion bodies. In spinal cord neurons of the pre-symptomatic L84V SOD1 transgenic mice, we observed aberrant aggregation of electron-dense rough ER around the peri-nuclear region with numerous free ribosomes, which were suspected to be producing mutant SOD1 (Fig. 7). This suggests that the aberrant SOD1 fibrils observed in spinal neurons of these mice at later

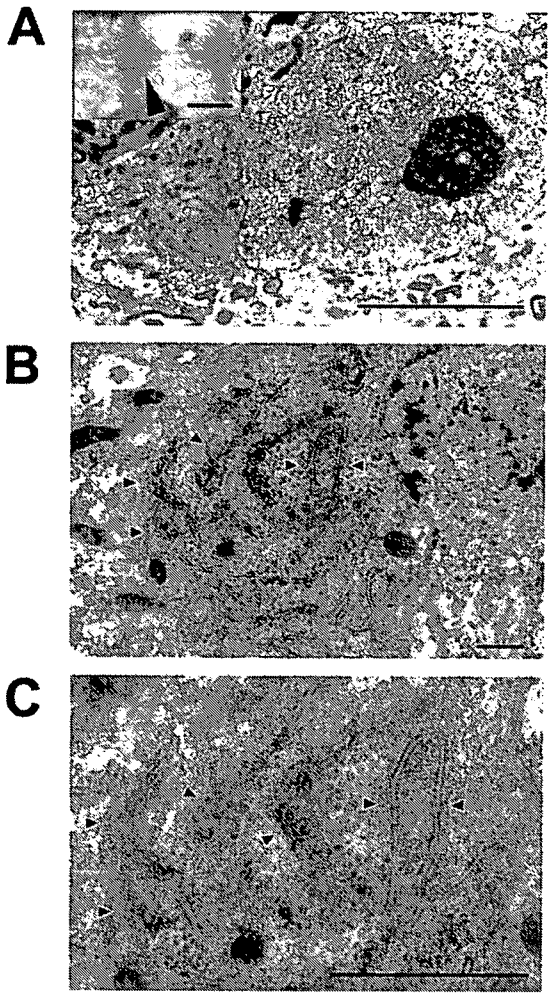

Figure 7. ER shows abnormal aggregation with numerous free ribosomes in L84V SOD1 mouse at presymptomatic stage. (A–C) Electron micrographs of a neuron obtained from an L84V SOD1 transgenic mouse containing ER aggregates. The inset in (A) shows a cytoplasmic inclusion-like structure (arrowhead) stained with toluidine blue. (A) ×3500 (scale bars = 20 μm). (B) ×8000 (scale bar = 1 μm). (C) ×15000 (scale bar = 1 μm). Arrowheads indicate abnormal ER aggregates.

doi:10.1371/journal.pone.0001030.g007